JACS
JOURNAL OF THE AMERICAN CHEMICAL SOCIETY
pubs.acs.org/JACS
Article

IR-VUV Photoionization Spectra of Hydrated BaOH Reveal Base Dissociation in Growing Water Clusters

Wenhui Yan, Shuai Jiang, Shangdong Li, Jianxing Zhuang, Ailin Wang, Hua Xie, Gang Li,* and Ling Jiang

Cite This: J. Am. Chem. Soc. 2026, 148, 3026−3033
Read Online
ACCESS | Metrics & More | Article Recommendations | Supporting Information

ABSTRACT: Investigating the dissociation of base in a microhydration environment is important for revealing various fundamental physical and chemical processes. In this study, neutral open-shell $BaOH(H_2O)_n$ (n = 1−5) clusters were characterized by size-specific infrared-vacuum ultraviolet photoionization spectroscopy combined with quantum chemical calculations and ab initio molecular dynamics simulations. The results show that the Ba−OH bond is undissociated for n = 1 and 2, and the transition from contact ion pair (CIP) to solvent-shared ion pair (SIP) spontaneously starts at n = 3. The present findings clarify the previous debate that BaOH shows no sign of dissociation even at n = 5. This work reveals the microscopic mechanisms of base dissolution processes and lays a solid foundation for broader application across systems.

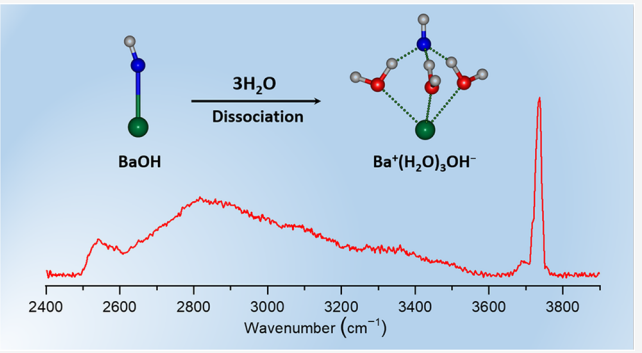

INTRODUCTION

Dissolution of bases in water is an elementary process in acid−base chemistry. The initial hydration and dissociation process of the base plays an important role in batteries and medicine.[1−3] Detailed investigations of structural evolution of base−water clusters enable us to isolate and comprehend specific phenomena like hydrogen bonding, proton transfer, electron delocalization, and electrostatic interactions, with nuances that may typically be obscured in the intricate bulk solvent environments.[4,5]

Solvation is defined by the characteristics of solute−solvent interactions and frequently entails a structural rearrangement of both entities. Notably, the basic question of how many water molecules are necessary to begin the dissociation process is still an open issue.[6−12] In recent decades, many efforts have been undertaken to reveal the dissociation of acids and salts by a step addition of water molecules.[13,14] In the case of HCl microhydration, infrared (IR) spectroscopy of helium droplets indicated that the fourth water molecule is responsible for triggering the so-called aggregation-induced dissociation of the HCl molecules, resulting in the formation of the charge-separated solvent-shared ion pair (SIP) $H_3O^+(H_2O)_3Cl^-$.[15,16] With high-resolution rotational spectroscopy, a significant breakthrough revealed that the contact ion pair of $H_3O^+Cl^-$ is spontaneously formed within the hydrogen-bonding networks of book at n = 5.[17] For the microsolvation process of sulfuric acid, the negative mass spectroscopy combined with density functional theory (DFT) calculation revealed that the initiation of the ionic dissociation of sulfuric acid and the formation of ion-pair (H_3O^+-HSO_4^-) structure in the neutral $H_2SO_4(H_2O)_n$ clusters emerges with $n \geq 5$ water molecules.[18−20] Analogously, many theoretical[21−23] and experimental[24−28] studies have been performed to investigate the number of water molecules required to induce contact ion pair (CIP) to solvent-separated ion pair (SSIP) transition in the microsolvation processes of salts. Despite the fact that these works provide insights into the solvation of acids and salts, experimental studies of solvation processes of bases are scarce, leaving the microscopic solvation mechanism unknown.

In this work, microhydrated $BaOH(H_2O)_n$ clusters were used as an example for IR spectroscopic studies on the microscopic solvation of neutral open-shell species. The BaOH system establishes its intrigue through two dimensions: (1) the unpaired electron of neutral BaOH and (2) the highly ionic character of Ba−OH bond.[29] As the number of water molecules increases, the ionization energy of open-shell $BaOH(H_2O)_n$ presents an opposite trend to that of closed-shell $MOH(H_2O)_n$ (M = alkali metal).[30−36] Investigation of stepwise microhydration of BaOH is highly desired to provide a distinctive opportunity to elucidate the interactions between the open-shell entities and the water molecules in terms of electrostatic and inductive contributions. Here, we report the

Received: August 28, 2025
Revised: January 2, 2026
Accepted: January 6, 2026
Published: January 13, 2026

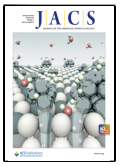

https://doi.org/10.1021/jacs.5c15032
J. Am. Chem. Soc. 2026, 148, 3026−3033

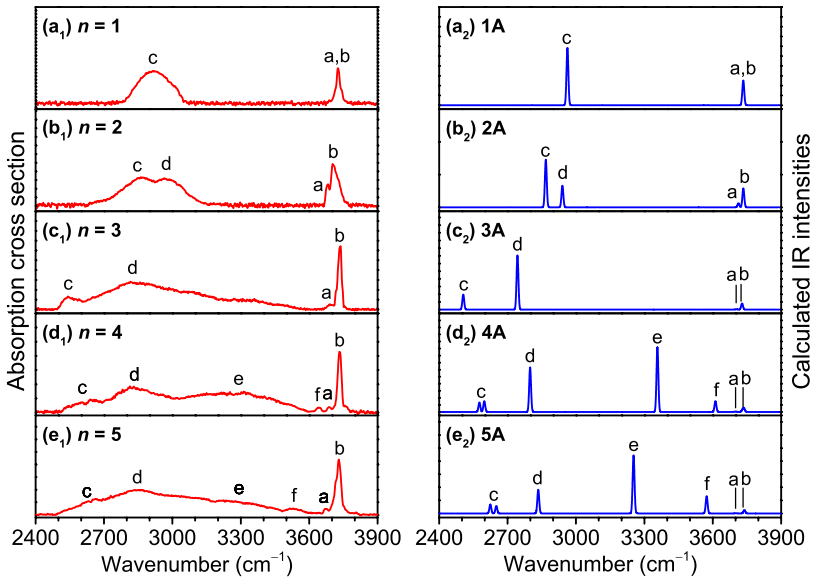

Figure 1. Experimental IR-VUV photoionization spectra of neutral $BaOH(H_2O)_n$ (n = 1−5). Calculated IR spectra of the lowest-energy isomers (nA) of neutral $BaOH(H_2O)_n$ (n = 1−5). Calculations were performed at the MP2(full)/aug-cc-pVTZ(O, H)/def2-TZVPP(Ba) level of theory, with the harmonic frequencies scaled by 0.951.[41]

Table 1. Experimental Vibrational Frequencies and Band Assignments of Neutral $BaOH(H_2O)_n$ (n = 1−5)

label	n = 1	n = 2	n = 3	n = 4	n = 5	assignment
a	3727	3682	3687	3686	3674	hydrogen-donor-free OH stretching mode of the O(1)H group
b	3727	3702	3737	3732	3730	hydrogen-donor-free OH stretching mode of the O(m)H (m = 2−4) groups
c	2913	2861	2542	2607 2639	2633 2663	nondegenerate a-type (m = 2 and 4)/degenerate e-type (m = 3) hydrogen-bonded OH stretching mode of the O(m)H (m = 2−4) groups
d		2963	2817	2814	2866	nondegenerate a-type hydrogen-bonded OH stretching mode of the O(m)H (m = 2−4) groups
e				3313	3235	nondegenerate a-type hydrogen-donor-free OH stretching mode of the O(m)H (m = 5 and/or 6) groups
f				3642	3516	nondegenerate a-type hydrogen-donor-free OH stretching mode of the O(m)H (m = 5 and/or 6) groups

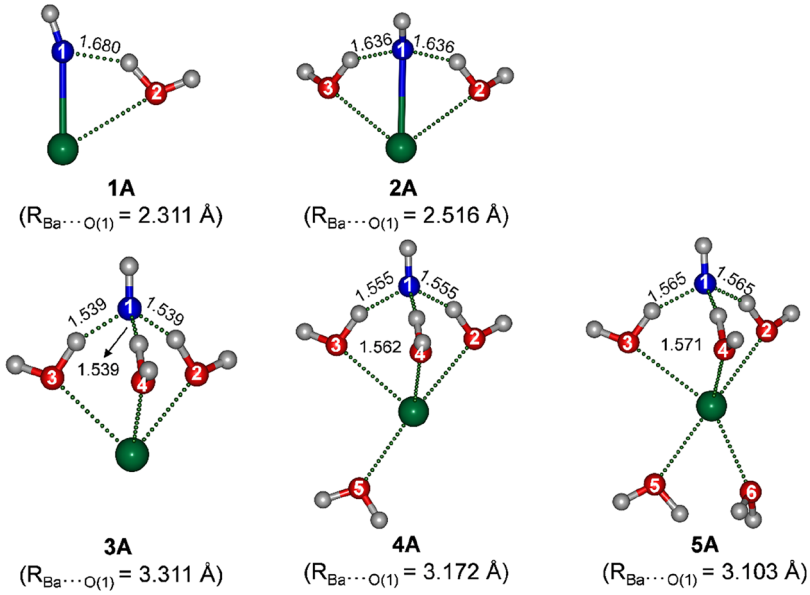

Figure 2. Optimized geometries of isomers nA (n = 1−5) at the MP2(full)/aug-cc-pVTZ(O, H)/def2-TZVPP(Ba) (abbreviated as MP2/AVTZ) level of theory (O, red; H, gray; Ba, Olive). The O atom derived from BaOH is indicated in all structures. Atoms are labeled for discussion. The lengths (Å) for the intermolecular hydrogen bonds and Ba−O distances (in parentheses) for the complexes are indicated.

size-specific infrared-vacuum ultraviolet (IR-VUV) photoionization spectra of neutral $BaOH(H_2O)_n$ (n = 1−5) clusters. The analyses of the BaOH hydration structures were conducted with the aid of quantum chemical calculations and ab initio molecular dynamics (AIMD) simulations. The dissociation mechanism of BaOH in water has been proposed.

https://doi.org/10.1021/jacs.5c15032
J. Am. Chem. Soc. 2026, 148, 3026−3033

RESULTS AND DISCUSSION

IR Spectra of $BaOH(H_2O)_n$ (n = 1−5)

A brief description of experimental and theoretical methods is given below, and further details are provided in the Supporting Information (SI). With the IR-VUV apparatus,[37,38] neutral $BaOH(H_2O)_n$ (n = 1−5) and BaO_3H_6 clusters were generated via laser vaporization supersonic expansion of a He/H_2O mixture. The neutral clusters were first irradiated with tunable IR light to cause vibrational predissociation and then photoionized by a 193 nm VUV light. The IR-VUV photoionization spectra were measured in the difference mode of operation (IR laser on minus IR laser off). The IR power dependence of the signal was measured to ensure a linear relationship between the predissociation yield and the photon flux. Geometry optimizations and vibrational analyses were carried out by using the Gaussian 16 package.[39] The AIMD simulations at finite temperatures were performed in the CP2K package.[40] The experimental IR-VUV photoionization spectra of neutral $BaOH(H_2O)_n$ (n = 1−5) clusters are presented in Figure 1a_1−e_1, with vibrational frequencies and band assignments in Table 1. The lowest-energy isomers of $BaOH(H_2O)_n$ (n = 1−5) (labeled 1A−5A) were obtained at the MP2(full)/aug-cc-pVTZ(O, H)/def2-TZVPP(Ba) (hereafter MP2/AVTZ) level and are depicted in Figure 2, with their calculated spectra in Figure 1a_2−e_2. Comparison of the experimental and theoretical band positions is given in Tables S1 and S2, respectively. The calculations successfully reproduce the core experimental spectral features.

In the high-frequency region (3650−3750 cm^{-1}) of calculated IR spectra (Figure 1a_2−e_2), the bands assigned to non-hydrogen-donor OH stretching vibrations exhibit systematic evolution. Specifically, the calculated peak for the hydrogen-donor-free OH stretch of the O(1)H group (labeled band a) progressively red-shifts with increasing hydration: starting at 3735 cm^{-1} for n = 1, decreasing to 3712 cm^{-1} for n = 2, and stabilizing between 3703 and 3701 cm^{-1} for n = 3−5 (Tables S1 and S2). This trend closely matches the experimental observations (n = 1:3727 cm^{-1}; n = 2:3682 cm^{-1}; n = 3:3687 cm^{-1}; n = 4:3686 cm^{-1}; n = 5:3674 cm^{-1}). Similarly, the free OH stretches of water O(m)H groups (m = 2−4) (band b) are calculated to be in the 3728−3740 cm^{-1} region. This includes a doublet at 3734/3735 cm^{-1} for n = 2 and multiple structures for n = 3−5 (e.g., 3738/3739/3740 cm^{-1} for n = 5). The agreement with experimental values (n = 1:3727 cm^{-1}; n = 2:3702 cm^{-1}; n = 3:3737 cm^{-1}; n = 4:3732 cm^{-1}; n = 5:3730 cm^{-1}) further validates the structural motifs of the clusters.

Within the hydrogen-bonding sensitive region (2500−3400 cm^{-1}), the evolution of spectral features directly reflects the changes of the intracluster hydrogen-bonding network structures. In particular, the experimental bands in the 2500−2700 cm^{-1} region start to appear in the n = 3 spectrum, indicative of a structural transformation. Indeed, the calculated peaks for the hydrogen-bonded OH stretching modes of O(m)H groups (m = 2−4) (band c) undergo a significant red shift with increasing water molecules: from 2962 cm^{-1} (n = 1) and 2868 cm^{-1} (n = 2) down to 2506 cm^{-1} (n = 3). For $n \geq 4$, peak splitting emerges due to the hydrogen-bonding network complexity (n = 4:2576/2598 cm^{-1}; n = 5:2624/2651 cm^{-1}), mirroring the experimental spectra which show the same trend at corresponding positions (n = 1:2913 cm^{-1}; n = 2:2861 cm^{-1}; n = 3:2542 cm^{-1}; n = 4:2607/2639 cm^{-1}; n = 5:2633/2663 cm^{-1}). In addition, the nondegenerate a-type hydrogen-bonded OH stretches ($n \geq 2$) (band d) exhibit the calculated peak positions decreasing from 2940 cm^{-1} (n = 2) to 2743 cm^{-1} (n = 3), followed by a slight recovery for n = 4 (2799 cm^{-1}) and n = 5 (2835 cm^{-1}). Their experimental counterparts (n = 2:2963 cm^{-1}; n = 3:2817 cm^{-1}; n = 4:2814 cm^{-1}; n = 5:2866 cm^{-1}) likewise display a distinct "V-shaped" trend, which is a sharp initial decrease followed by a gradual rise, indicative of dynamic changes in the hydrogen-bonding symmetry with accompanying solvation shell restructuring.

For higher-hydration clusters ($n \geq 4$), the nondegenerate a-type hydrogen-donor-free OH stretches of outer-shell water O(m)H groups (m = 5 and/or 6) (bands e and f) are identified. In the calculated spectra, for n = 4, band e and band f are located at 3357 cm^{-1} and 3612 cm^{-1}, respectively. For n = 5, band e is split into components at 3253 cm^{-1} and 3265 cm^{-1}, while band f appears at 3573−3574 cm^{-1}. The overall agreement of these theoretical results with experimental observations (n = 4: band e at 3313 cm^{-1}, band f at 3642 cm^{-1}; n = 5: band e at 3235 cm^{-1}, band f at 3516 cm^{-1}) is reasonable to confirm the spatial orientation differentiation and local environmental heterogeneity of water molecules within the solvation shell.

For isomer 1A, the water bending vibrational mode and hydrogen-bonded OH stretching mode of the O(2)H group are calculated to be 1554 and 2962 cm^{-1} at the MP2/AVTZ level of theory, respectively. The gap of the water bend overtone (3108 cm^{-1}) and hydrogen-bonded OH stretching mode of the O(2)H group (2962 cm^{-1}) is 146 cm^{-1}, which is covered in the span (300 cm^{-1}) of band c. Thus, the water bend overtone may also contribute to the broad feature of experimental band c. Note that the interaction between the waters and the BaOH unit may exist in these clusters, for which anharmonic quantum mechanical calculations are expected to elucidate the origin of the couplings of different vibrational motions.[42−44]

Hydration-Induced Ba−OH Dissociation

This study systematically investigates the structural evolution and electronic properties of neutral hydrated clusters $BaOH(H_2O)_n$ (n = 1−5), elucidating the dissociation mechanism of the BaOH radical under sequential hydration. Structural analyses (Figures 2 and S2−S6) reveal a distinct transition: for hydration numbers n = 1 and 2, the lowest-energy isomers (1A and 2A) retain the ionic bond framework of the BaOH radical, with water molecules directly interacting via O−H···O hydrogen bonds, which are consistent with previous calculations.[30,31] In contrast, for $n \geq 3$, the lowest-energy isomers (3A−5A) exhibit a fundamental structural shift in which the Ba atom coordinates directly with multiple water molecules, while the OH group is separated via a hydrogen-bonding network, forming SIP. This structural reorganization correlates strongly with the elongation of the Ba···O(1)H distance (Table S3): $R_{Ba\cdots O(1)H}$ increases progressively from 2.331 Å (n = 1) to 2.515 Å (n = 2) and undergoes a pronounced elongation to 3.311 Å at n = 3, showing a net increase of 0.98 Å from n = 1 to n = 3. Subsequent elongation becomes moderate for n = 4 (3.172 Å) and n = 5 (3.103 Å) ($\Delta R_{Ba\cdots O(1)H}$ < 0.2 Å), indicating structural saturation and dynamic equilibrium. In contrast, previous studies suggested that the lowest-energy isomer for n = 3 had a CIP (Ba−OH undissociated) structure,[30,31] which is different from this work. The lowest-energy isomers for n = 4 and 5 were predicted to have the SIP

https://doi.org/10.1021/jacs.5c15032
J. Am. Chem. Soc. 2026, 148, 3026−3033

(Ba···OH dissociated) structures,[30] which are in accord with our present results.

Electronic structure analysis further elucidates the underlying driving mechanisms. Mulliken charge populations (Table S3) show the predominantly ionic character of $Ba^{+}-OH^{-}$ across the $n = 1-5$ clusters. Upon sequential hydration, the net negative charge accumulated on the solvent shell progressively increases (n = 1: −0.05; n = 2: −0.20; n = 3: −0.33), attenuating the Ba−OH electrostatic attraction. In the meantime, the Mulliken charge on the O(1)H group in n = 1−3 is −0.77, −0.66, and −0.55, respectively, indicating the trend to reduce polarization and to facilitate Ba−OH bond elongation and rupture. Remarkably, for $n \geq 3$, the Mulliken charge on O(1)H is alleviated at −0.55, signifying charge saturation. Such charge changes are consistent with the remarkable red shift of band c from n = 2 to n = 3, supporting the structural transformation with the SIP formation. The positive charge on the Ba increases to > + 1.00 for 4A and 5A, driven by direct water coordination and charge transfer to outer-shell molecules (e.g., $H_2O(5)/H_2O(6)$), enhancing the SIP stability. The results of energy decomposition analysis (EDA) (Table S4) support the electrostatic and polarization interaction mechanisms. With the stepwise hydration of water molecules from 1A to 3A, the electrostatic attraction (ΔE_{els}) in the Ba−OH fragment progressively weakens (−52.76 → −37.99 → −11.48 kcal/mol). From 3A to 5A, the variation in ΔE_{els} becomes less than 3 kcal/mol. Concurrently, the orbital interaction energy (ΔE_{orb}) exhibits a similar decreasing trend from 1A to 3A (−134.59 → −111.54 → −46.48 kcal/mol). Note that the terms ΔE_{els} and ΔE_{orb} are components of the total interfragment interaction energy (ΔE_{int}), as defined within the sobEDA framework.[45] ΔE_{int} represents the energy change when fragments combine in the geometry of the complex, encompassing electrostatic, exchange, Pauli repulsion, orbital interaction (including polarization), and correlation/dispersion contributions. ΔE_{int} is not equivalent to the bond dissociation energy. The actual binding energy includes the deformation energy required to distort the isolated fragments to their geometry in the complex. Therefore, the observed trends in ΔE_{els} and ΔE_{orb} reflect the structural evolution of specific interaction components within the complex and not the total energy required to break the bond. The SIP formation in n = 3 is supported through multiple evidence: (i) energetics: the global minimum structure 3A with a dissociated Ba−OH is more favorable than the next energetically higher structure 3B with a nondissociated Ba−OH by 1.69 kcal/mol at the MP2/AVTZ level; (ii) kinetics: the intrinsic reaction coordinate calculation reveals a very small barrier of 2.69 kcal/mol for the 3B → 3A isomerization (Figure 3). This barrier is readily surmountable under laser vaporization source conditions, and the transformation is facilitated by a hydrogen-transfer (specific to the hydrogen of the H_2O molecule) competent hydrogen-bonding network, indicating that Ba−OH dissociation is both thermodynamically favorable (exothermic) and kinetically accessible.

The pronounced ionic nature of the Ba−OH bond governs the solvation behavior, rendering BaOH susceptible to dissociation.[29] The unpaired electron maintains nonbonding character, suppressing delocalization. The dissociation of the Ba−OH bond at n = 3 is driven synergistically: charge transfer attenuates electrostatic attraction while the hydrogen-bonding network reorganization facilitates the hydrogen transfer, yielding stable SIP. With the combination of experimental spectra and theoretical calculations, our results demonstrate that three water molecules are able to dissociate BaOH. This finding clarifies the previous argument that BaOH shows no sign of complete dissociation even at n = 5.[29,30] The present discovery is reminiscent of a central question in metal solvation science that is the determination of the minimum number of water molecules required to dissociate the cation and anion of a metal salt molecule.[24]

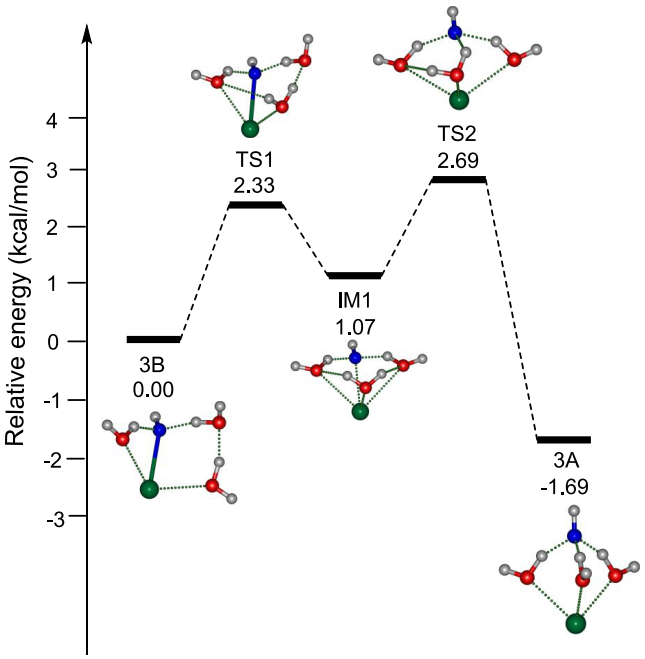

Figure 3. Potential energy profiles of the 3B → 3A isomerization calculated at the MP2(full)/aug-cc-pVTZ(O, H)/def2-TZVPP(Ba) level of theory. Energies are given in kcal/mol. The relative energies are calculated by the Gibbs free energies at 150 K.

AIMD Simulation Validation

The $BaOH(H_2O)_3$ cluster emerges as the critical midway, featuring the transition from CIP to SIP in neutral open-shell alkaline-earth hydration systems. Its extensive hydrogen-bonding interactions manifest experimentally as pronounced spectral broadening within the hydrogen-bonded OH stretching region. A multitiered computational strategy was employed for a better understanding of experimental spectral features. The above harmonic vibrational analyses based on the equilibrium geometries provide preliminary spectral assignments of vibrational fundamentals. Subsequently, AIMD simulations were performed to incorporate anharmonicity and thermal effects, with the attempt to interpret the experimental spectral broadening and relative band intensities. To systematically elucidate the discrepancies between harmonic predictions and experimental observations, AIMD simulations were conducted under a series of temperatures (from 50 to 200 K). As demonstrated in Figure 4, the AIMD simulated spectrum accumulated over 150 ps at 150 K reasonably reproduces the overall line shape of the experimental spectrum. This approach addresses the inherent limitations of the static harmonic approximation for flexible hydrogen-bonded clusters, which fails to capture the experimentally observed variations in peak intensity distributions and band broadening arising from atomic thermal motions.

https://doi.org/10.1021/jacs.5c15032
J. Am. Chem. Soc. 2026, 148, 3026−3033

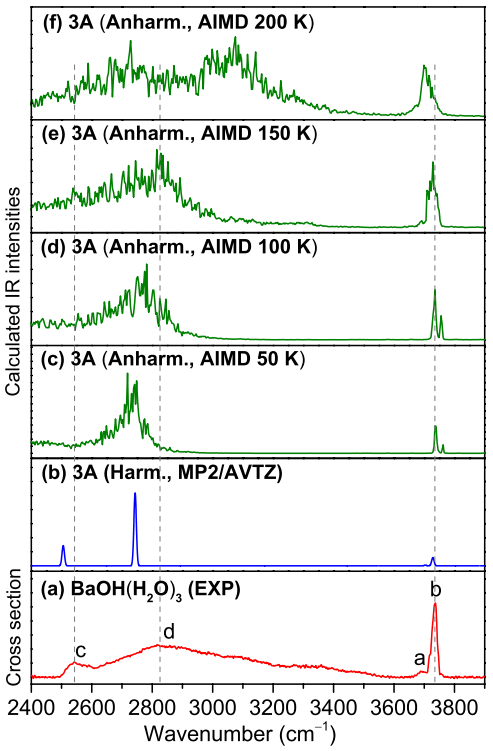

Figure 4. Comparison of experimental IR-VUV photoionization spectrum of neutral $BaOH(H_2O)_3$ (a) and MP2/AVTZ calculated harmonic IR spectrum of isomer 3A (b) and AIMD simulated spectra at 50, 100, 150, and 200 K (c–f) of isomer 3A.

Analysis for the 3A cluster reveals that at 50 K (Figure 4c), hydrogen-bonded OH stretching modes (bands c and d) exhibit initial broadening. Upon increasing the temperature to 150 K (Figure 4e), spectral broadening intensifies markedly, and the AIMD simulated spectrum achieves the best agreement with experimental data across the entire spectral range in terms of band positions and relative intensities. The plot of vibrational density of states obtained from the AIMD simulations (Figure S7) reveals that the spectral feature in the 3000–3600 cm^{-1} region of $BaOH(H_2O)_3$ mainly arises from the combined contributions of hydrogen-bonded O–H stretching modes of the O5H6, O7H4, and O9H11 groups. The AIMD simulated spectra of isomers 2A, 4A, and 5A provide further support for the above discussions (Figures S8 and S9). Statistical mechanical evidence for the dynamic stability of the hydrogen-bonding network is derived from AIMD trajectory analysis of the 3A cluster at 150 K (Figure S10). The distributions of both Ba···O(m) (m = 2–4) distances (Figure S10a–d) and O(1)···H(x) (x = 5–7) hydrogen-bond lengths (Figure S10e–f) exhibit Gaussian characteristics, with fluctuation amplitudes consistently confined within the 0.4–0.6 Å range. This verifies the structural robustness of the 3A configuration during the finite-temperature dynamics.

It is noted that the AIMD temperature, controlled via atomic kinetic energy, does not directly equate to the experimental condition, where laser-induced heating in the vaporization source elevates the temperature beyond that of a pure supersonic expansion. Furthermore, the presented AIMD simulations lack explicit zero-point vibrational energy corrections and quantum nuclear effects.[40,46−48] Despite these approximations, AIMD simulations help to capture the thermally induced and atomic-motion-dominated broadening mechanisms operated in the actual system. While the AIMD simulations did not fully reproduce the present experimental spectra, further improvement of the theoretical model is expected.

Theoretical Verification of the Reaction Pathway

Building upon prior studies demonstrating that the barium-water reaction generates the radical product BaOH + H selectively via the electronic excitation of the barium atom ($Ba(^1D_2)$),[49] we proposed the formation pathway of $BaOH(H_2O)_3$ through IR-VUV photoionization spectroscopy and potential energy surface calculations, for which mechanisms are not exclusive. The experimental IR-VUV photoionization spectrum of the BaO_3H_6 cluster exhibits a high degree of agreement with the theoretical IR spectrum of the $HBaOH(H_2O)_2$ structure (Figure 5 and Table S5). Energetically, this

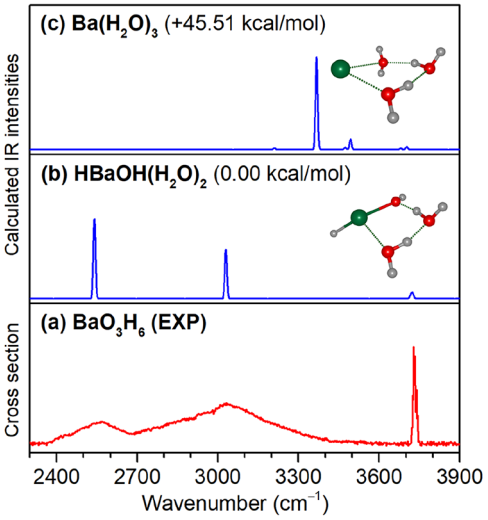

Figure 5. Comparison of the experimental IR-VUV photoionization spectrum of neutral BaO_3H_6 and calculated IR spectra of $HBaOH(H_2O)_2$ and $Ba(H_2O)_3$. Calculations were performed at the MP2(full)//aug-cc-pVTZ(O, H)/def2-TZVPP(Ba) level of theory, with the harmonic frequencies scaled by 0.951 (O, red; H, light gray; Ba, olive).

insertion structure is significantly more stable (by 45.51 kcal/mol) than the competing isomer $Ba(H_2O)_3$, which can be spontaneously converted to $HBaOH(H_2O)_2$ via a small barrier of 9.51 kcal/mol (Figure S11). Notably, although dehydrogenation of $HBaOH(H_2O)_2$ to form $BaOH(H_2O)_2$ + H is endothermic (51.09 kcal/mol), an entropy-driven process of $Ba(^1D_2)$ + $4H_2O$ reactions in high-temperature plasma environments of a laser-evaporation source can facilitate this conversion. Subsequent hydration of $BaOH(H_2O)_2$ readily leads to the formation of $BaOH(H_2O)_3$ (Figure S11). Importantly, all remaining steps along this reaction pathway are thermodynamically favorable (exothermic) and kinetically accessible (Table S6). Although the barrier of the BaH_2O → HBaOH isomerization is 15.98 kcal/mol (Figure S11), BaH_2O was not detected in the present experiments, which could be due to the small barrier of the $Ba(H_2O)_3$ → $HBaOH(H_2O)_2$ isomerization (9.51 kcal/mol) and the large exothermicity of the $Ba(^1D_2)$ + $4H_2O$ → $BaOH(H_2O)_3$ + H process.

The $BaOH(H_2O)_3$ cluster plays a dual role: it serves as the terminal product of the radical hydration pathway while

https://doi.org/10.1021/jacs.5c15032
J. Am. Chem. Soc. 2026, 148, 3026−3033

simultaneously acting as the dynamic nexus for solvation structural reorganization, specifically, the transition from CIP to SIP. Its extensive hydrogen-bonding interactions, evidenced by pronounced broadening in the experimental IR-VUV photoionization spectrum, drive ion separation through thermally induced atomic motions. By integrating IR-VUV photoionization spectroscopy (validating the H atom transfer mechanism), potential energy surface mapping (locating intermediates), and anharmonic molecular dynamics simulations (reproducing hydrogen-bond fluctuations), this study establishes a reasonable correlation between the electronic state of the reactant, reaction pathway, and the evolution of solvation structure. This integrated approach provides a new paradigm for elucidating ion-pair evolution mechanisms in solvated systems. The present findings have demonstrated that the early stage solvation dynamics of closed-shell systems could be accessed through their open-shell precursors, offering a microscopic prelude to the macroscopic mechanism of the solution phase. This work also substantiates that accurate interpretation of experimental spectra of solvated species requires the combination of high-level quantum chemical calculations, ab initio molecular dynamics simulations, and anharmonic algorithm.

CONCLUSIONS

We utilized the IR-VUV method to obtain IR action spectra of neutral $BaOH(H_2O)_n$ (n = 1−5) in the OH stretch vibrational region. Combined with quantum chemical harmonic calculations and AIMD anharmonic simulations, the structures of $BaOH(H_2O)_n$ clusters were determined. AIMD simulations reasonably interpret the broadening of the experimental spectral bands in the context of hydrogen-bond fluctuations. Our studies show that the solvent-shared ion-pair types of structures start to appear at n = 3. The dissociation of BaOH in water is initiated by Ba^+-OH^- electrostatic and polarization interactions: charge transfer reduces electrostatic attraction, while the reconfiguration of the hydrogen-bonding network facilitates hydrogen transfer. The present system serves as a model for describing the interaction between the open-shell entities and the water molecules in terms of electrostatic and inductive effects and opens new avenues for understanding the early stage of solvation processes of a wide variety of closed-shell systems.

ASSOCIATED CONTENT

Supporting Information

The Supporting Information is available free of charge at https://pubs.acs.org/doi/10.1021/jacs.5c15032.

Detailed experimental and theoretical methods; time-of-flight mass spectrum (Figure S1); comparison of experimental IR-VUV photoionization spectrum of $BaOH(H_2O)_n$ (n = 1−5) and calculated spectra of their low-lying isomers (Figures S2−S6); dipole time-correlation function spectrum and density of state plots of isomer 3A (Figure S7); comparison of experimental IR-VUV photoionization spectra of $BaOH(H_2O)_n$ (n = 2−5) and AIMD simulated spectra at 150 K of isomers 2A-5A (Figure S8); comparison of experimental IR-VUV photoionization spectrum of neutral $BaOH(H_2O)_2$ with MP2/AVTZ calculated harmonic spectrum of isomer 2A and AIMD simulated spectra of isomer 2A (Figure S9); normal distribution of Ba···O and O(1)···H distances (Figure S10); potential energy profiles of the reactions of $Ba(^1D_2)$ with H_2O (Figure S11); comparison of the experimental and theoretical band positions of $BaOH(H_2O)_n$ (n = 1−5) (Tables S1 and S2); Ba···O(1)H distances and Mulliken charges of OH bond in isomers nA (n = 1−5) (Table S3); sobEDA analysis results of Ba···O(1)H for isomers nA (n = 1−5) (Table S4); comparison of experimental and theoretical band positions of BaO_3H_6 (Table S5); reaction energies of the formation of $HBaOH(H_2O)_2$ and $BaOH(H_2O)_3$ (isomer 3A) (Table S6); dissociation energies of isomers 1A−5A (Table S7); and cartesian coordinates (PDF)

AUTHOR INFORMATION

Corresponding Author

Gang Li − *State Key Laboratory of Chemical Reaction Dynamics and Dalian Coherent Light Source, Dalian Institute of Chemical Physics, Chinese Academy of Sciences, Dalian 116023, China; University of Chinese Academy of Sciences, Beijing 100049, China;* orcid.org/0000-0001-5984-111X; Email: gli@dicp.ac.cn

Authors

Wenhui Yan − *State Key Laboratory of Chemical Reaction Dynamics and Dalian Coherent Light Source, Dalian Institute of Chemical Physics, Chinese Academy of Sciences, Dalian 116023, China; University of Chinese Academy of Sciences, Beijing 100049, China*

Shuai Jiang − *State Key Laboratory of Chemical Reaction Dynamics and Dalian Coherent Light Source, Dalian Institute of Chemical Physics, Chinese Academy of Sciences, Dalian 116023, China; University of Chinese Academy of Sciences, Beijing 100049, China*

Shangdong Li − *State Key Laboratory of Chemical Reaction Dynamics and Dalian Coherent Light Source, Dalian Institute of Chemical Physics, Chinese Academy of Sciences, Dalian 116023, China; University of Chinese Academy of Sciences, Beijing 100049, China*

Jianxing Zhuang − *State Key Laboratory of Chemical Reaction Dynamics and Dalian Coherent Light Source, Dalian Institute of Chemical Physics, Chinese Academy of Sciences, Dalian 116023, China; University of Chinese Academy of Sciences, Beijing 100049, China*

Ailin Wang − *State Key Laboratory of Chemical Reaction Dynamics and Dalian Coherent Light Source, Dalian Institute of Chemical Physics, Chinese Academy of Sciences, Dalian 116023, China; University of Chinese Academy of Sciences, Beijing 100049, China*

Hua Xie − *State Key Laboratory of Chemical Reaction Dynamics and Dalian Coherent Light Source, Dalian Institute of Chemical Physics, Chinese Academy of Sciences, Dalian 116023, China; University of Chinese Academy of Sciences, Beijing 100049, China;* orcid.org/0000-0003-2091-6457

Ling Jiang − *State Key Laboratory of Chemical Reaction Dynamics and Dalian Coherent Light Source, Dalian Institute of Chemical Physics, Chinese Academy of Sciences, Dalian 116023, China; University of Chinese Academy of Sciences, Beijing 100049, China; Hefei National Laboratory, Hefei 230088, China;* orcid.org/0000-0002-8485-8893

Complete contact information is available at: https://pubs.acs.org/10.1021/jacs.5c15032

https://doi.org/10.1021/jacs.5c15032
J. Am. Chem. Soc. 2026, 148, 3026−3033

Notes

The authors declare no competing financial interest.

■ ACKNOWLEDGMENTS

The authors gratefully acknowledge the staff members of the Dalian Coherent Light Source (31127.02.DCLS) for technical support and assistance in data collection. This work was supported by the National Natural Science Foundation of China (Nos. 22373102, 22125303, 92361302, 22273101, 22288201, and 21327901), the Strategic Priority Research Program of the Chinese Academy of Sciences (XDB0970100), the National Key Research and Development Program of China (No. 2021YFA1400501), the Innovation Program for Quantum Science and Technology (No. 2021ZD0303304), the Dalian Institute of Chemical Physics (DICP I202437), the Chinese Academy of Sciences (No. GJJSTD20220001), and the International Partnership Program of CAS (121421KYSB20170012).

■ REFERENCES

(1) Wakihara, M.; Yamamoto, O. *Lithium Ion Batteries: Fundamentals and Performance*; Iop Publishing Ltd, 2008.
(2) Whittingham, M. S. Lithium Batteries and Cathode Materials. *Chem. Rev.* **2004**, *104*, 4271−4301.
(3) Schrauzer, G. N.; Klippel, K. F. *Lithium in Biology and Medicine: New Applications and Developments*; Vch Pub, 1991.
(4) Campargue, R. *Atomic and Molecular Beams: The State of the Art*; Springer, 2012; Vol. *2000*.
(5) Stace, A. Chemistry - Cluster solutions. *Science* **2001**, *294*, 1292−1293.
(6) Rognoni, A.; Conte, R.; Ceotto, M. How many water molecules are needed to solvate one? *Chem. Sci.* **2021**, *12*, 2060−2064.
(7) Mishima, O.; Stanley, H. E. The relationship between liquid, supercooled and glassy water. *Nature* **1998**, *396*, 329−335.
(8) Errington, J. R.; Debenedetti, P. G. Relationship between structural order and the anomalies of liquid water. *Nature* **2001**, *409*, 318−321.
(9) Marx, D. Throwing tetrahedral dice. *Science* **2004**, *303*, 634−636.
(10) Angell, C. A. Insights into phases of liquid water from study of its unusual glass-forming properties. *Science* **2008**, *319*, 582−587.
(11) Fournier, J. A.; Johnson, C. J.; Wolke, C. T.; Weddle, G. H.; Wolk, A. B.; Johnson, M. A. Vibrational spectral signature of the proton defect in the three-dimensional $H^+(H_2O)_{21}$ cluster. *Science* **2014**, *344*, 1009−1012.
(12) Tielrooij, K. J.; Garcia-Araez, N.; Bonn, M.; Bakker, H. J. Cooperativity in ion hydration. *Science* **2010**, *328*, 1006−1009.
(13) Leopold, K. R. Hydrated acid clusters. *Annu. Rev. Phys. Chem.* **2011**, *62*, 327−349.
(14) Hurley, S. M.; Dermota, T. E.; Hydutsky, D. P.; Castleman, A. W. Dynamics of hydrogen bromide dissolution in the ground and excited states. *Science* **2002**, *298*, 202−204.
(15) Gutberlet, A.; Schwaab, G.; Birer, O.; Masia, M.; Kaczmarek, A.; Forbert, H.; Havenith, M.; Marx, D. Aggregation-induced dissociation of $HCl(H_2O)_4$ below 1 K: the smallest droplet of acid. *Science* **2009**, *324*, 1545−1548.
(16) Forbert, H.; Masia, M.; Kaczmarek-Kedziera, A.; Nair, N. N.; Marx, D. Aggregation-induced chemical reactions: Acid dissociation in growing water clusters. *J. Am. Chem. Soc.* **2011**, *133*, 4062−4072.
(17) Xie, F.; Tikhonov, D. S.; Schnell, M. Electric nuclear quadrupole coupling reveals dissociation of HCl with a few water molecules. *Science* **2024**, *384*, 1435−1440.
(18) Bandy, A. R.; Ianni, J. C. Study of the hydrates of H_2SO_4 using density functional theory. *J. Phys. Chem. A* **1998**, *102*, 6533−6539.
(19) Re, S.; Osamura, Y.; Morokuma, K. Coexistence of neutral and ion-pair clusters of hydrated sulfuric acid $H_2SO_4(H_2O)_n$ (n = 1−5) - A molecular orbital study. *J. Phys. Chem. A* **1999**, *103*, 3535−3547.
(20) Lengyel, J.; Pysanenko, A.; Farnik, M. Electron-induced chemistry in microhydrated sulfuric acid clusters. *Atmos. Chem. Phys.* **2017**, *17*, 14171−14180.
(21) Belch, A. C.; Berkowitz, M.; McCammon, J. A. Solvation structure of a sodium chloride ion pair in water. *J. Am. Chem. Soc.* **1986**, *108*, 1755−1761.
(22) Woon, D. E.; Dunning, T. H. The pronounced effect of microsolvation on diatomic alkali-halides: *Ab initio* modeling of $MX(H_2O)_n$ (M = Li, Na; X = F, Cl; n = 1−3). *J. Am. Chem. Soc.* **1995**, *117*, 1090−1097.
(23) Siu, C.-K.; Fox-Beyer, B. S.; Beyer, M. K.; Bondybey, V. E. Ab initio molecular dynamics studies of ionic dissolution and precipitation of sodium chloride and silver chloride in water clusters, $NaCl(H_2O)_n$ and $AgCl(H_2O)_n$, n = 6, 10, and 14. *Chem. - Eur. J.* **2006**, *12*, 6382−6392.
(24) Li, R.-Z.; Liu, C.-W.; Gao, Y. Q.; Jiang, H.; Xu, H.-G.; Zheng, W.-J. Microsolvation of LiI and CsI in water: Anion photoelectron spectroscopy and *ab initio* calculations. *J. Am. Chem. Soc.* **2013**, *135*, 5190−5199.
(25) Ault, B. S. Infrared spectra of argon matrix-isolated alkali halide salt/water complexes. *J. Am. Chem. Soc.* **1978**, *100*, 2426−2433.
(26) Dedonder-Lardeux, C.; Grégoire, G.; Jouvet, C.; Martrenchard, S.; Solgadi, D. Charge separation in molecular clusters: Dissolution of a salt in a salt-$(solvent)_n$ cluster. *Chem. Rev.* **2000**, *100*, 4023−4037.
(27) Zhang, Q.; Carpenter, C. J.; Kemper, P. R.; Bowers, M. T. On the dissolution processes of Na_2I^+ and $Na_3I_2^+$ with the association of water molecules: Mechanistic and energetic details. *J. Am. Chem. Soc.* **2003**, *125*, 3341−3352.
(28) Mizoguchi, A.; Ohshima, Y.; Endo, Y. Microscopic hydration of the sodium chloride ion pair. *J. Am. Chem. Soc.* **2003**, *125*, 1716−1717.
(29) Rossa, M.; Cabanillas-Vidosa, I.; Pino, G. A.; Ferrero, J. C. New determination of the adiabatic ionization potential of the BaOH radical from laser photoionization-molecular beam experiments and *ab initio* calculations. *J. Chem. Phys.* **2012**, *136*, No. 064303.
(30) Cabanillas-Vidosa, I.; Rossa, M.; Pino, G. A.; Ferrero, J. C.; Cobos, C. J. Hydration of barium monohydroxide in $(H_2O)_{1-3}$ clusters: Theory and experiment. *J. Phys. Chem. A* **2013**, *117*, 4997−5006.
(31) Rossa, M.; Ferrero, J. C.; Cabanillas-Vidosa, I.; Cobos, C. J. Theoretical study of the microscopic solvation of alkali and alkaline-earth monohydroxides in $(H_2O)_m$ ($m \leq 3$) clusters. *Chem. Phys. Lett.* **2015**, *620*, 19−24.
(32) Odde, S.; Pak, C.; Lee, H. M.; Kim, K. S.; Mhin, B. J. Aqua dissociation nature of cesium hydroxide. *J. Chem. Phys.* **2004**, *121*, 204−208.
(33) Odde, S.; Lee, H. M.; Kolaski, M.; Mhin, B. J.; Kim, K. S. Dissolution of a base (RbOH) by water clusters. *J. Chem. Phys.* **2004**, *121*, 4665−4670.
(34) Veerman, A.; Lee, H. M.; Kim, K. S. Dissolution nature of the lithium hydroxide by water molecules. *J. Chem. Phys.* **2005**, *123*, No. 084321.
(35) Kumar, A.; Park, M.; Huh, J. Y.; Lee, H. M.; Kim, K. S. Hydration phenomena of sodium and potassium hydroxides by water molecules. *J. Phys. Chem. A* **2006**, *110*, 12484−12493.
(36) Roy, D. R. Theoretical study of microscopic solvation of NaOH in water: $NaOH(H_2O)_n$, n = 1−10. *Chem. Phys.* **2012**, *407*, 92−96.
(37) Zhang, B.; Yu, Y.; Zhang, Z.; Zhang, Y.-Y.; Jiang, S.; Li, Q.; Yang, S.; Hu, H.-S.; Zhang, W.; Dai, D.; et al. Infrared spectroscopy of neutral water dimer based on a tunable vacuum ultraviolet free electron laser. *J. Phys. Chem. Lett.* **2020**, *11*, 851−855.
(38) Li, G.; Wang, C.; Li, Q.; Zheng, H.; Wang, T.; Yu, Y.; Su, M.; Yang, D.; Shi, L.; Yang, J.; et al. Infrared + vacuum ultraviolet two-color ionization spectroscopy of neutral metal complexes based on a tunable vacuum ultraviolet free-electron laser. *Rev. Sci. Instrum.* **2020**, *91*, No. 034103.
(39) Frisch, M. J.; Trucks, G. W.; Schlegel, H. B.; Scuseria, G. E.; Robb, M. A.; Cheeseman, J. R.; Scalmani, G.; Barone, V.; Petersson,

https://doi.org/10.1021/jacs.5c15032
J. Am. Chem. Soc. 2026, 148, 3026−3033

G. A.; Nakatsuji, H.et al. *Gaussian 16, Revision A. 03, Gaussian, Inc.*, Gaussian 2016.
(40) VandeVondele, J.; Krack, M.; Mohamed, F.; Parrinello, M.; Chassaing, T.; Hutter, J. Quickstep: fast and accurate density functional calculations using a mixed Gaussian and plane waves approach. *Comput. Phys. Commun.* **2005**, *167*, 103−128.
(41) Johnson, R. D. NIST computational chemistry comparison and benchmark database 2006 https://cccbdb.nist.gov/.
(42) Qu, C.; Bowman, J. M. Quantum approaches to vibrational dynamics and spectroscopy: Is ease of interpretation sacrificed as rigor increases? *Phys. Chem. Chem. Phys.* **2019**, *21*, 3397−3413.
(43) Sibert, E. L. Modeling vibrational anharmonicity in infrared spectra of high frequency vibrations of polyatomic molecules. *J. Chem. Phys.* **2019**, *150*, No. 090901.
(44) Zhang, B.; Yang, S.; Huang, Q.-R.; Jiang, S.; Chen, R.; Yang, X.; Zhang, D. H.; Zhang, Z.; Kuo, J.-L.; Jiang, L. Deconstructing vibrational motions on the potential energy surfaces of hydrogen-bonded complexes. *CCS Chem.* **2020**, *2*, 829−835.
(45) Lu, T.; Chen, Q. Simple, Efficient, and Universal Energy Decomposition Analysis Method Based on Dispersion-Corrected Density Functional Theory. *J. Phys. Chem. A* **2023**, *127*, 7023−7035.
(46) VandeVondele, J.; Mohamed, F.; Krack, M.; Hutter, J.; Sprik, M.; Parrinello, M. The influence of temperature and density functional models in ab initio molecular dynamics simulation of liquid water. *J. Chem. Phys.* **2005**, *122*, No. 014515.
(47) Barducci, A.; Bonomi, M.; Parrinello, M. Metadynamics. *WIREs Comput. Mol. Sci.* **2011**, *1*, 826−843.
(48) Li, H.; Kong, X.; Jiang, L.; Liu, Z.-F. Size-dependent formation of an ion pair in $HSO_4^-(H_2O)_n$: A molecular model for probing the microsolvation of acid dissociation. *J. Phys. Chem. Lett.* **2019**, *10*, 2162−2169.
(49) Davis, H. F.; Suits, A. G.; Lee, Y. T.; Alcaraz, C.; Mestdagh, J. M. State specific reactions of Ba($^1S_0$) and Ba($^1D_2$) with water and methanol. *J. Chem. Phys.* **1993**, *98*, 9595−9609.

https://doi.org/10.1021/jacs.5c15032
J. Am. Chem. Soc. 2026, 148, 3026−3033